HIGH-BRIGHTNESS RACETRACK MICROTRON INJECTOR*

R.A. Barday†, V.P. Gorbachev‡, A.M. Gorokhov†, E.A. Knapp, V.I. Shvedunov†, N.P. Sobenin§, A.A. Sulimov§, W.P. Trower, A.A. Vetrov†, and D.A. Zayarny#, World Physics Technologies, Blacksburg VA 24060 USA

Abstract

Our **R**ace**T**rack **M**icrotron will produce electron beams with energies up to 35 MeV, ~5 mm×mrad normalized emittance, bunch charge in excess of 150 pC, and rates up to 150 Hz [1]. Its 5 MeV injector consists of a 1.6 MeV **R**adio-**F**requency laser stimulated photocathode electron gun and a 3.4 MeV linac. We describe the injector and RF-system performance, as well as the beam diagnostics.

1 DESCRIPTION

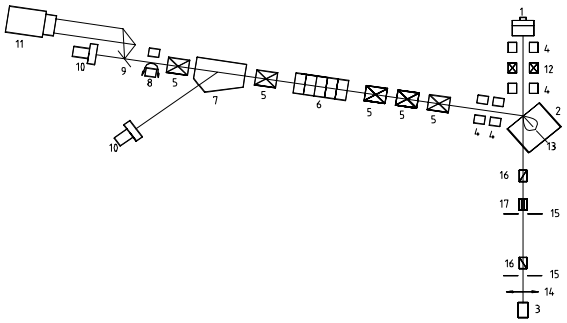

Figure 1: RTM injector schematic.

Our injector, seen in Fig. 1, has a 1+1/2 cell RF-gun (1) whose barium impregnated tungsten cathode is illuminated by 500 ps, 248 nm eximer laser pulses (3) focused by a lens (14) on an aperture (15) and truncated from its initial 8 ns duration by an electro-optical modulator (17) and polarizers (16). A variable-gradient rare-earth α-magnet (2) [2] bunches the beam while a collimating slit (13) truncates its energy spectrum. The beam is accelerated to 5 MeV by a 5-cell linac (6). Horizontal and vertical steering coils (4), solenoid lenses (12), and quadrupoles (5) provide beam transport. We monitor the beam with a 45º magnetic spectrometer (7), a fast transformer beam current monitor (8), a CCD-based transition radiation detector (9,11) and a Faraday cup (10).

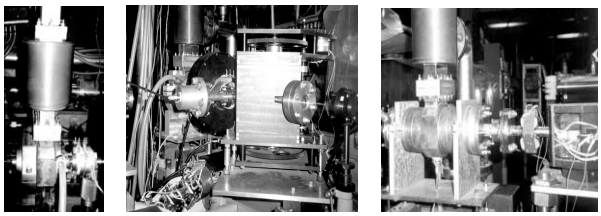

Figure 2: RF-gun/vacuum port, α-magnet, and linac.

Table 1: RF-gun and linac parameters.

	RF-gun	Linac
RF frequency (MHz)	2,856	2,856
Loaded quality factor	5,300	7,100
Shunt impedance (MΩ)	5	16
Coupling factor	1.06	1.08

The injector elements are shown in Fig. 2, the gun and linac parameters are listed in Table 1, and their field distributions are seen in Fig. 3.

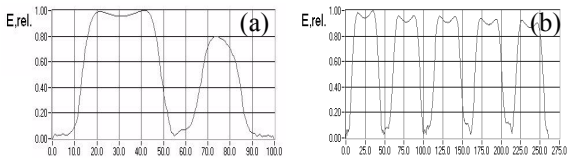

Figure 3: On-axis electric field: (a) gun and (b) linac.

Electrons from the 2,856 MHz RF-gun, seen in Fig. 4, enter the α-magnet and exit in dispersion-free longitudinally compressed bunches with a central energy of 1.6 MeV. We can adjust the 400 G/cm field gradient by ±10% to match the RTM acceptance. The nominal 3 mm wide collimating slit allows electrons to pass whose energy deviates by less than ±0.08 MeV from the selected central energy of 1.41 to 1.73 MeV. In our experiments we increase the slit width up to 4.5 mm and for some measurements we remove the slits.

*Work supported in part by U.S. Department of Energy 50043-98-II.
†Permanent address: Nuclear Physics Institute, Moscow State University, 119899 Moscow, Russia.
‡Permanent address: Institute of Mechanics and Physics, 410026 Saratov, Russia.
§Permanent address: Moscow Engineering and Physics Institute, 115409 Moscow, Russia.
#Permanent address: Lebedev Physical Institute, 117924 Moscow, Russia.

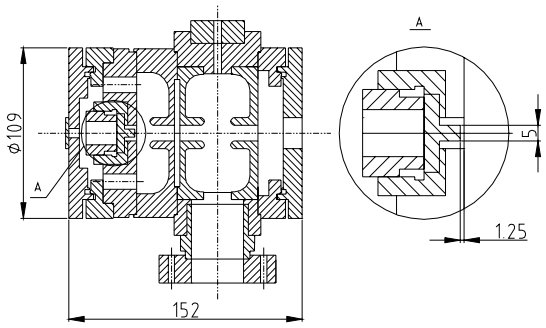

Figure 4: RF-gun elevation view.

1.1 RF system

We drive our RF-system, seen in Fig. 5, with an adjustable frequency master oscillator that provides a laser system synchronization signal and a nominal 2,856 MHz signal stable to 10^{-7} that can be amplified to a 200 W pulse power. Part of the main signal enters a directional coupler (DC1) and is passed to phase detectors (PD4-6), which control the gun and linac phases. An amplified RF signal feeds the klystron through an attenuator, which regulates the power and locks out the klystron when RF faults occur. RF power from the 6 MW klystron producing 6 μs, 150 Hz pulses is distributed to the gun, the linac, and the RTM accelerating structure through two 3 dB directional waveguide couplers (DC2-3), while 0.2-10 dB adjustable attenuators (A2-4) determine the power levels. Phase shifter (Φ1-2) ranges exceed 360˚.

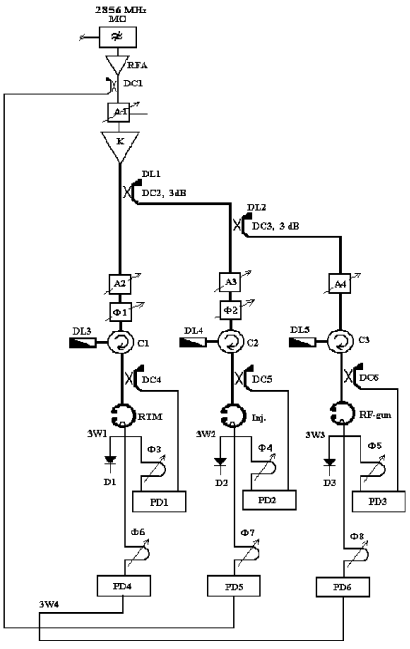

Figure 5: RTM injector.

The klystron is protected from reflected power damage by circulators placed before the gun and the linac. After passing through the vacuum window, the RF power enters the linac. We install a coupling loop with 3-way power dividers in the gun, the linac, and the RTM structures (3W1-3) to provide a RF signal to the pulse amplitude controlling coaxial RF diodes (D1-3), to the phase controlling detectors (PD1-3) whose operating points are determined by phase shifters (Φ3-8), and to the resonance frequency controlling analogue phase detectors (PD4-6).

1.2 Laser system

Our laser system includes the eximer laser, a 1.5 m focal length lens, diaphragms, an electro-optical modulator, and two polarizers. Since our W-Ba photocathode has only a ~2 eV work function and a quantum efficiency of less than 10^{-3}, the laser pulse energy per RF period at the cathode needed to extract ~1 nC of charge must exceed 5 mJ. Our 248 nm Kr/F laser produces 30 mJ in 8 ns pulses, as seen in Fig. 6(a), when measured with a vacuum photodiode. To produce ~500 ps pulses, we insert the electro-optical modulator, controlled by the pulses of Fig. 6(b), between crossed polarizers.

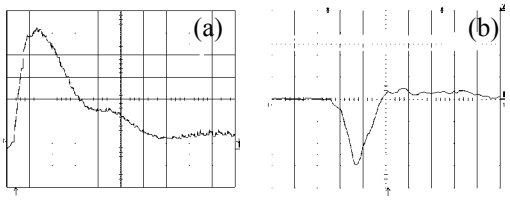

Figure 6: (a) Laser – 5 ns/div and (b) HV – 1 ns/div pulse.

1.3 Beam diagnostics

Our 50 Ω coaxial Faraday cup beam current monitor is connected to an 8 ns resolution preamplifier, as seen in Fig. 7 together with a typical beam pulse. Our non-intercepting beam current monitors have a 5.6 mV/mA sensitivity. We measure the beam energy and its spectrum with a 45º-dipole magnet in whose focal plane we install a 3 mm wide collimating slit. We measure the beam spot by transition radiation produced when it crosses a 20 μm thick aluminium foil placed at 45º to the beam and view it by a CCD camera.

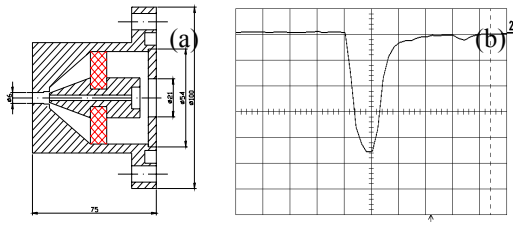

Figure 7: (a) Faraday cup and (b) beam pulse (b).

2 RESULTS

2.1 Thermionic RF gun operation

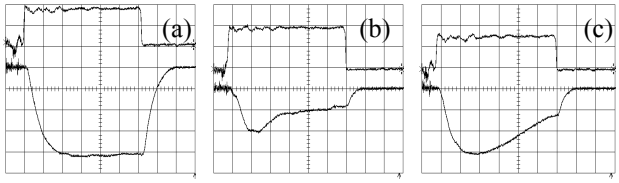

Figure 8: Klystron input (top) and gun diode (bottom) signals for (a) 0, (b) 1.2, and (c) 1 A cathode currents.

At low beam loading our RF-gun is almost critically coupled with the waveguide. Figure 8(a) shows a RF pulse when 0.4 MW is dissipated in the gun and the cathode heater current is zero. Holding the RF pulse constant while gradually increase the heater current, at 1.2 A the pulse amplitude abruptly drops (from increased beam loading) and the pulse shape becomes distorted (from back-bombarding electrons) as seen in Fig. 8(b). Decreasing the heater current to 1 A improves the pulse shape, seen in Fig. 8(c), as the thermionic emission ceases. We will not operate in the thermionic mode.

2.2 Laser stimulated RF gun operation

Figure 9 shows the gun field under cathode irradiation with ~1 A of cathode heater current and 0.7 MW of RF power. Of the 30 mJ laser pulse energy, ~8 mJ arrives at the cathode when the modulator is switched off. The charge released during the 8 ns pulse consumes up to 20% of the stored gun energy.

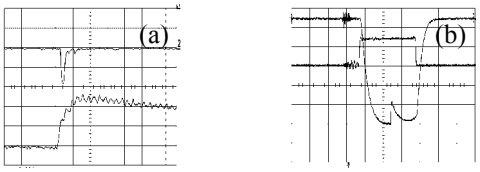

Figure 9: Gun field with (a) Faraday cup and (b) klystron signals.

We install a RF probe in the 2nd gun ½-cell to measure the gun field with time seen in Fig. 9(a) at 50 ns/div where the upper curve is the Faraday cup signal and the lower is the RF diode signal. Both cells are strongly coupled so that 10 ns after irradiation the 2nd cell field slowly decays and the ripple is from energy being redistributed between the two cells. The RF-gun structure field is restored through the feeding waveguide with a ~0.6 μs time constant.

After calibrating the RF diode with the power dissipated in the gun walls, we measure the gun quality factor and the average beam energy exiting the gun and estimate that ~22 bunches accelerated in gun during 8 ns contained ~1 nC/bunch. Figure 9(b) shows the gun field with the klystron input signal at 2 μs/div when the cathode is irradiated. The cathode quantum efficiency is at least 7.5×10^{-5} with a 1 A cathode heater current.

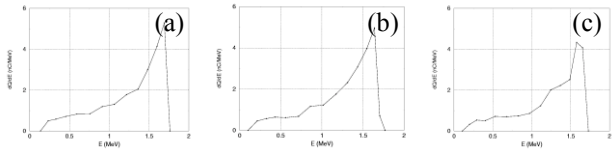

Figure 10: Bunch energy spectra: (a) 1, (b) 6, and (c) 12.

Because many applications will operate in the multi-bunch mode, we simulate the energy decrease of successive bunches due to the decrease in stored energy. The calculated energy spectra for the 1st, 6th, and 12th bunch at the gun exit with 2.7 nC/bunch are seen in Fig. 10. We estimate that the maximum bunch energy decreases by 15 keV/period/nC or 330 keV for 1 nC of accelerated charge over 22 periods. Thus, depending on the collimating slit width, only a fraction of high charge bunches pass through the α-magnet.

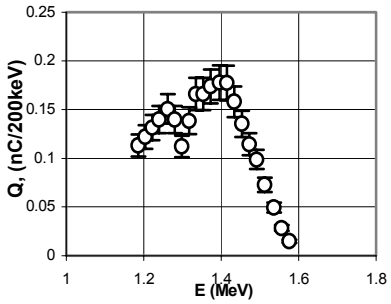

Figure 11: Energy spectrum after α–magnet.

We measure the energy spectrum with a moveable 4.5 mm wide slit collimator installed in the α-magnet vacuum chamber and record the Faraday cup charge when 0.4 MW is dissipated in the walls, as seen in Fig. 11.

REFERENCES

[1] A.S. Alimov, K. Halbach, E.A. Knapp, D.V. Kostin, G.A. Novikov, V.I. Shvedunov, N.P. Sobenin, and W.P. Trower, "Generating High-Brightness Electron Beams," in Proc. 1999 Particle Accelerator Conf., A. Luccio and W. MacKay, eds. (IEEE, Piscataway, 1999) v. 4, p. 2301.

[2] V.S. Skachkov, "A Variable Gradient Rare Earth Permanent α-Magnet," in Proc. 2000 European Particle Accelerator Conf., J.L. Laclare, W. Mitaroff, Ch. Petit-Jean-Genaz, J. Poole, and M. Regler eds. (World Scientific, Singapore, 2000) p. 2122.